arXiv:nucl-ex/0312018v1 17 Dec 2003

Experimental study of μ–atomic and μ–molecular processes in pure helium and deuterium–helium mixtures

V.M. Bystritsky,[1,*] V.F. Boreiko,[1] W. Czapliński,[2] M. Filipowicz,[3] V.V. Gerasimov,[1]
O. Huot,[4] P.E. Knowles,[4] F. Mulhauser,[4,†] V.N. Pavlov,[1] N.P. Popov,[2,‡] L.A. Schaller,[4]
H. Schneuwly,[4] V.G. Sandukovsky,[1] V.A. Stolupin,[1] V.P. Volnykh,[1] and J. Woźniak[2]
[1] *Joint Institute for Nuclear Research, Dubna 141980, Russia*
[2] *University of Mining and Metallurgy, Fac. Phys. Nucl. Techniques, PL–30059 Cracow, Poland*
[3] *University of Mining and Metallurgy, Fac. of Fuels and Energy, PL–30059 Cracow, Poland*
[4] *Department of Physics, University of Fribourg, CH–1700 Fribourg, Switzerland*
(Dated: February 8, 2008)

We present experimental results of μ–atomic and μ–molecular processes induced by negative muons in pure helium and helium–deuterium mixtures. The experiment was performed at the Paul Scherrer Institute (Switzerland). We measured muonic x–ray K series transitions relative intensities in $(\mu^{3,4}\mathrm{He})^*$ atoms in pure helium as well as in helium–deuterium mixture. The muon stopping powers ratio between helium and deuterium atoms and the $d\mu^3\mathrm{He}$ radiative decay probability of for two different helium densities in $\mathrm{D}_2+{}^3\mathrm{He}$ mixture were also determined. Finally, the $\mathrm{q}_{1s}^{\mathrm{He}}$ probability for a $d\mu$ atom formed in an excited state to reach the ground state was measured and compared with theoretical calculations using a simple cascade model.

PACS numbers: 34.70.+e, 36.10.Dr, 39.10.+j, 82.30.Fi
Keywords: muonic atom, muon transfer, helium, deuterium, muon stopping power, muonic x rays

I. INTRODUCTION

The experimental study of atomic and molecular processes induced by negative muons captured in hydrogen and helium provides a test of many–body calculations [1] comprising different methods of atomic, molecular, and nuclear physics. In spite of about 50 years of experimental [2, 3, 4, 5, 6] and theoretical [7, 8, 9, 10, 11] studies for processes occurring in helium and deuterium, as well as helium–deuterium mixtures, there exist still some open questions. The most important are listed here:

- direct atomic muon capture in h–He mixtures ($h = \mathrm{H}_2, \mathrm{D}_2, \mathrm{T}_2$ and $\mathrm{He} = {}^3\mathrm{He}, {}^4\mathrm{He}$);
- initial population of μh and μHe excited states for various deexcitation processes of muonic atoms (e.g., Stark mixing, Auger and Coulomb deexcitation processes [12, 13, 14, 15, 16]);
- muon transfer between excited states of μh and μHe [16, 17, 18, 19, 20];
- the probability q_{1s} to reach the μh ground state in a h–He mixture [16, 17, 20, 21, 22, 23];
- ground state muon transfer from μh to helium via the intermediate $2p\sigma$ molecular state, $h\mu$He [24, 25, 26, 27, 28], and the subsequent decay to the unbound $1s\sigma$ state [2, 20, 22, 29, 30].

In the case of a deuterium–helium mixture the $(d\mu\mathrm{He})^*$ molecule, created in $d\mu+\mathrm{He}$ collisions, has three possible decay channels:

$$\begin{aligned} d\mu + \mathrm{He} \xrightarrow{\lambda_{d\mu\mathrm{He}}} [(d\mu\mathrm{He})^* e] &\xrightarrow{\lambda_\gamma} [(\mu\mathrm{He})^+_{1s} e] + d + \gamma \quad \text{(1a)} \\ &\xrightarrow{\lambda_p} [(\mu\mathrm{He})^+_{1s} e] + d \quad \text{(1b)} \\ &\xrightarrow{\lambda_e} (\mu\mathrm{He})^+_{1s} + d + e\,. \quad \text{(1c)} \end{aligned}$$

Here, λ_γ is the $(d\mu\mathrm{He})^*$ molecular decay channel for the 6.85 keV γ–ray emission, λ_e for the Auger decay, and λ_p for the break–up process. The $(d\mu\mathrm{He})$ molecule is formed, with a rate $\lambda_{d\mathrm{He}}$, in either a $J=0$ or a $J=1$ rotational state (J denotes the total angular momentum of the three particles). The $J=1$ state is mostly populated at slow $d\mu$–He collisions. The $J=1 \rightarrow J=0$ deexcitation due to inner or outer Auger transition is also possible [31, 32, 33]. In principle it competes with the decay processes of Eq. (1), and can be followed by another decay due to nuclear deuterium–helium fusion from the $J=0$ state [34, 35].

In this paper we present experimental results for fundamental characteristics of μ–atomic (MA) and μ–molecular (MM) processes in a $\mathrm{D}_2+{}^3\mathrm{He}$ mixture, namely the muon stopping power ratio, the $\mathrm{q}_{1s}^{\mathrm{He}}$ probability, the radiative branching ratio for the radiative decay of the $(d\mu^3\mathrm{He})^*$ molecule (1a), and delayed Lyman series transitions in μHe atoms for two different target densities and at nearly constant helium concentrations. Results for relative intensities of $\mu\mathrm{He}\,K$ series transitions in pure ${}^{3,4}\mathrm{He}$ and $\mathrm{D}_2+{}^3\mathrm{He}$ for different target densities are also presented.

---

[*] Corresponding author; Electronic address: bystvm@nusun.jinr.ru

[†] Present address: University of Illinois at Urbana–Champaign, Urbana, Illinois 61801, USA

[‡] Visiting Professor

II. EXPERIMENTAL CONDITIONS

A study of MA and MM processes mentioned above requires the simultaneous use of miscellaneous detectors appropriate for the detection of the muon beam, the muonic x rays of μh and μHe atoms (formed in the target due to direct muon capture by the correspondent nuclei or due to muon transfer from hydrogen to helium), products of nuclear reactions occurring in $\mu h-$He complexes, and muon decay electrons. Detection of the latter is necessary not only for yield normalization but also for background reduction. This was realized by requesting that the muon survives atomic and molecular processes. Thus, muon decay electrons were detected within a certain time interval after the principal particle detection. For a precise measurement of the characteristics of MA and MM processes the detection system and the associated electronics should posses high energy and time resolutions.

The experiment was performed at the Paul Scherrer Institute (PSI) at the μE4 muon channel. It is described in details in Refs. [36, 37, 38]. A schematic muon eyes view of the setup is given in Fig. 1.

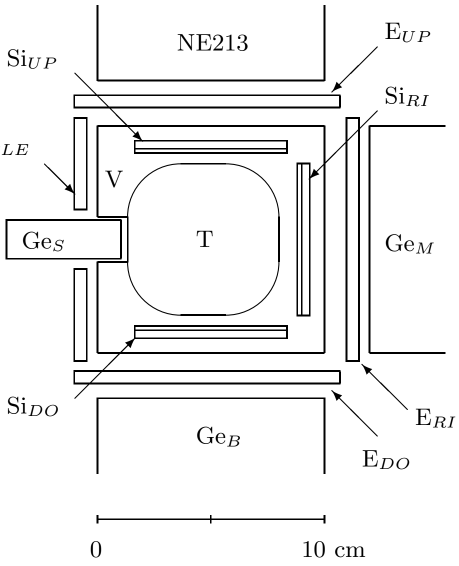

FIG. 1: Scheme of the experimental setup. The view is that of the incoming muon.

TABLE I: Experimental conditions, such as temperature, pressure, density, and helium concentration. The last column presents the number of muon stops in the gas.

Run	Gas	Temp. [K]	Pressure [atm]	φ [LHD]	c_{He} [%]	N_{stop} [10^6]
I	^{3}He	32.9	—	—	100	—
Ia			6.92	0.0363		640.4
Ib			6.85	0.0359		338.1
Ic			6.78	0.0355		375.3
Id			6.43	0.0337		201.7
II	^{4}He	—	—	—	100	—
IIa		20.3	12.55	0.1060		239.4
IIb		19.8	9.69	0.844		554.1
IIc		20.0	4.52	0.039		32.3
	$D_2 + {}^3$He	32.8	—	—	4.96	—
III			5.11	0.0585		4215.6
IV			12.08	0.1680		2615.4

The experimental setup was designed and developed to study nuclear reactions in charge asymmetric muonic molecules such as ($d\mu^3$He) [34, 35, 37, 39, 40, 41, 42, 43, 44]:

$$d\mu^3\mathrm{He} \rightarrow \alpha\,(3.66\,\mathrm{MeV}) + \mu + p\,(14.64\,\mathrm{MeV}). \qquad (2)$$

Charged muon–capture products were detected by three silicon telescopes located directly in front of the kapton windows but still within the cooled vacuum environment (Si_{UP}, Si_{RI}, and Si_{DO}). Muon decay electrons were detected by four pairs of plastic scintillator counters (E_{LE}, E_{UP}, E_{RI}, E_{DO}) placed around the target. The cryogenic target body was made of pure aluminium and had different kapton windows in order to detect in particular

- the $\sim$ 34 MeV/c momentum muon beam,
- the 6.85 keV γ rays emitted via the radiative decay given in Eq. (1a),
- the x–ray Lyman series transitions from the μHe deexcitation ($K\alpha$ at 8.2 keV, $K\beta$ at 9.6 keV, and $K\gamma$ at 10.2 keV).

The 0.17 cm^3 germanium detector (Ge_S) used for the γ and x–ray detection was placed just behind a 55 μm thick kapton window.

The experiment includes four groups of measurements as depicted in Table I. The first two groups, I and II, are ^{3}He and ^{4}He measurements at different temperatures and pressures. The remaining measurements, III and IV, were performed with $D_2 + {}^3$He mixtures at two different densities. The density φ is normalized to the liquid hydrogen density (LHD), $N_0 = 4.25 \times 10^{22}\,\mathrm{cm}^{-3}$. Run III was by far the longest run because its original purpose was to measure the fusion rate in the $d\mu^3$He molecule, Eq. (2), and the muon transfer rate $\lambda_{d^3\mathrm{He}}$ from $d\mu$ atoms to ^{3}He nuclei [37]. The germanium detector energy calibration was carried out during the data taking period using standard sources, namely ^{60}Co, ^{57}Co, ^{55}Fe, and ^{137}Cs.

III. METHOD OF THE MEASUREMENT

The MA and MM processes occurring in $D_2 + {}^3$He mixtures after the muon has stopped in a target volume is explained in detail in Ref [38]. The main characteristics are shown in Fig. 2. Depending on the time elapsed after

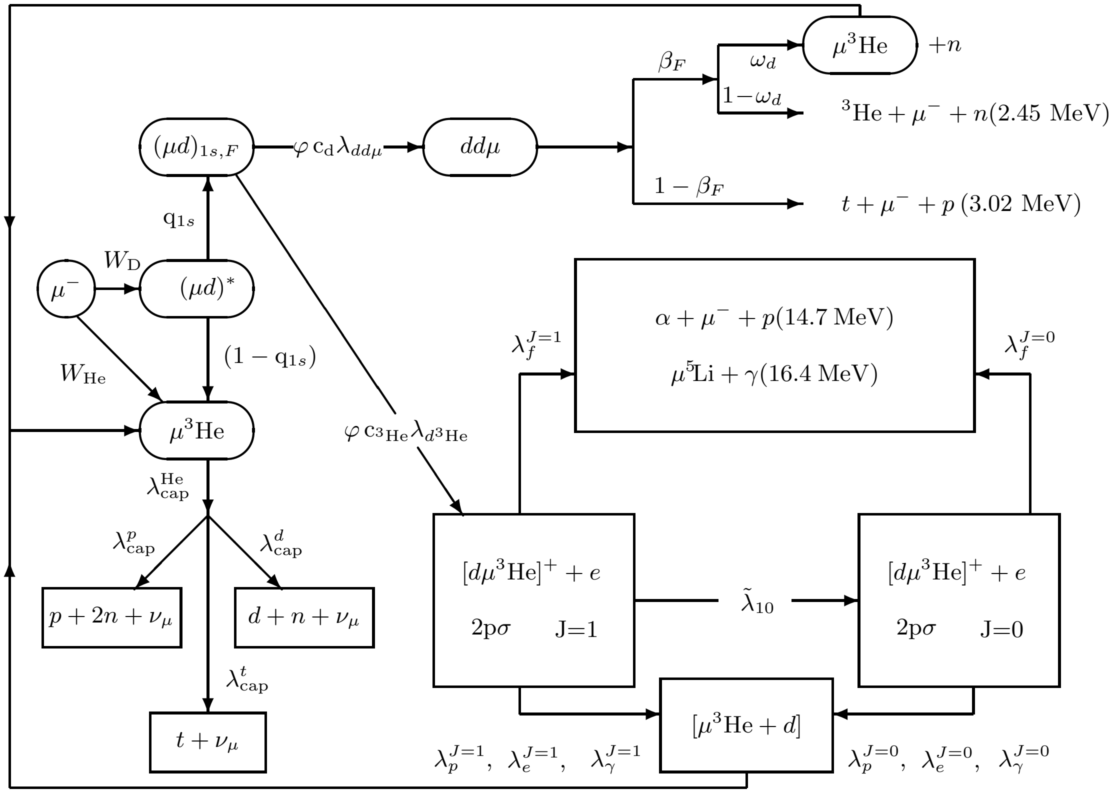

FIG. 2: Scheme of μ–atomic and μ–molecular processes in the D$_2$ + ^{3}He mixture. Details about all processes and rates are found in Ref. [37].

a muon stop in a mixture one can distinguish between prompt and delayed MA processes.

The following processes are considered as prompt ones:

- the slowing down of muons entering a target to velocities enabling an atomic capture into excited states of μh or μHe, with a characteristic moderation time $t_{mod} < 10^{-9}$ s for target densities $\varphi > 10^{-3}$ [7, 45, 46, 47, 48];
- the formation of excited muonic atoms, $(\mu h)^*$, $(\mu\mathrm{He})^*$, $t_{form} \sim 10^{-11}$ s [14];
- the cascade transitions in $(\mu h)^*$ and $(\mu\mathrm{He})^*$ muonic atoms, $t_{casc} \sim 10^{-11}$ s [49];
- the muon transfer from exited states of $(\mu h)^*$ to helium (occurring in D$_2$ + ^{3}He mixtures), $t \leq 10^{-10}$ s [17, 19, 20, 22].

The delayed processes are:

- the ground state muon transfer from muonic deuterium to helium [22, 28];
- the formation of excited $(d\mu^3\mathrm{He})^*$ molecules (with the subsequent prompt decay after about 10^{-11} s [29, 30]).

A. Pure helium

One of the main characteristics of MA processes occurring in pure helium are absolute and relative intensities of muonic K series x–ray transitions in $(\mu\mathrm{He})^*$ atoms. Their knowledge provides important information about the excited states initial population of the μHe atoms and the dynamics of deexcitation. According to the above given classification of MA processes and the conditions of runs I and II it is clear that only prompt K series transitions from μHe were observed. Events detected by the germanium detector within a time range $-30\,\mathrm{ns} \leq t_\gamma \leq 30\,\mathrm{ns}$ around time $t = 0$ (defined as the muon stop time) were classified as prompt. The chosen time range is a consequence of the detector and its related electronic time resolution. The relative intensities, I_x^{He}, of the Kx lines ($x \equiv \alpha, \beta, \gamma$) are:

$$I_x^{\mathrm{He}} = \frac{Y_x^{\mathrm{He}}}{Y_{tot}^{\mathrm{He}}} \qquad \text{with} \qquad \sum_{x=\alpha,\beta,\gamma} I_x^{\mathrm{He}} = 1\,, \tag{3}$$

where $Y_\alpha^{\mathrm{He}}, Y_\beta^{\mathrm{He}}, Y_\gamma^{\mathrm{He}}$ are the yields of μHe Kx lines with energies 8.17 keV, 9.68 keV, and 10.2 keV, respectively. These yields are determined as follows:

$$Y_x^{\mathrm{He}} = \frac{N_x^{\mathrm{He}}}{(1-\eta_x)\varepsilon_x}\,, \qquad Y_{tot}^{\mathrm{He}} = \sum_{x=\alpha,\beta,\gamma} Y_x^{\mathrm{He}} \tag{4}$$

with $Y_{tot}^{\rm He}$ being the total yield of all Kx lines. The quantities $N_x^{\rm He}$ are the prompt events numbers corresponding to the μHe Kx lines. η_x are the total attenuation coefficients of the corresponding Kx lines and ε_x are the corresponding detection efficiencies. The $I_\gamma^{\rm He}$ intensity is the cumulative photon yield of the Lyman series $n \geq 4$.

In fact, only detection efficiency ratios ($\varepsilon_{x\alpha} = \varepsilon_x/\varepsilon_\alpha$) are required for the determination of the relative intensities. Therefore Eq. (3) can be rewritten as

$$I_x^{\rm He} = \frac{N_x^{\rm He}}{N_{tot}^{\rm He}(1-\eta_x)\varepsilon_{x\alpha}}\,, \tag{5}$$

with

$$N_{tot}^{\rm He} = \sum_{x=\alpha,\beta,\gamma} \frac{N_x^{\rm He}}{(1-\eta_x)\varepsilon_{x\alpha}} \tag{6}$$

being the total yield normalized to the detection efficiency ε_α. This fact significantly increases the accuracy of $I_x^{\rm He}$ measured in experiment. The corresponding errors were mainly due to insufficient knowledge of the respective attenuation coefficients. One can expect, however, that attenuation coefficients, as compiled in Ref. [50], differ only slightly because the differences between energies of Kx lines ($\Delta E_{\beta-\alpha} = E(K\beta) - E(K\alpha) = 1.51$ keV, $\Delta E_{\gamma-\alpha} = E(K\gamma) - E(K\alpha) = 2.03$ keV) are relatively small. Recent experimental results also confirmed this assumption (see Refs. [20, 28]).

The detection efficiencies, ε_x are determined using Eqs. (3) and (4) via

$$\varepsilon_x = \frac{N_x^{\rm He}}{N_{\rm stop}^{\rm He} I_x^{\rm He}}\,, \tag{7}$$

where $N_{\rm stop}^{\rm He}$ is the number of muons stopping in helium, given in Table I. For an accurate determination of the K series transitions attenuation coefficient we performed Monte Carlo (MC) calculations taking into account the experimental geometry and all material layers placed between the x–ray emission and the germanium detector. The total attenuation coefficient η_x of each Kx line includes the x–ray attenuation while passing through the gas, the target and chamber kapton window, and through the germanium detector Be window taken from Ref. [51]. We obtained $\eta_\alpha = 0.156$, $\eta_\beta = 0.085$, and $\eta_\gamma = 0.075$.

A significant reduction of the germanium detector background was achieved by using delayed coincidences between x rays and electrons. This method is called the "del-e" criterion. Ground state muonic helium atoms disappear mainly by muon decay,

$$\mu^- \to e^- + \nu_\mu + \bar{\nu}_e\,, \tag{8}$$

and by nuclear muon capture (with proton, deuteron, or triton emission [38, 52, 53]). The average disappearance rate is

$$\lambda_{\rm He} = \lambda_0 + \lambda_{cap}^{\rm He} \approx 0.457 \times 10^6\,{\rm s}^{-1}\,, \tag{9}$$

where $\lambda_0 = 0.455 \times 10^6\,{\rm s}^{-1}$ and $\lambda_{cap}^{\rm He} = 2216(70)\,{\rm s}^{-1}$ [52]. Thus, delayed electrons were measured during a time interval corresponding to two μHe atom life times ($\tau_{\rm He} = 2.19\,\mu$s [54]).

The relative intensities of Kx lines, $I_{x-{\rm e}}^{\rm He}$, detected in coincidences with muon decay electrons, are given by

$$I_{x-{\rm e}}^{\rm He} = \frac{1}{\varepsilon_{\rm e} f_t} \frac{N_{x-{\rm e}}^{\rm He}}{N_{tot,{\rm e}}^{\rm He}(1-\eta_x)\varepsilon_{x\alpha}} \tag{10}$$

with

$$N_{tot,{\rm e}}^{\rm He} = \frac{1}{\varepsilon_{\rm e} f_t} \sum_{x=\alpha,\beta,\gamma} \frac{N_{x-{\rm e}}^{\rm He}}{(1-\eta_x)\varepsilon_{x\alpha}} \tag{11}$$

where $N_{x-{\rm e}}^{\rm He}$ are the number of events in pure helium detected by the germanium detector in coincidence with muon decay electrons within a fixed time interval $\Delta t = t_e - t_\gamma$, with t_γ and t_e the time of the germanium and decay electron counters, respectively. Both times are measured relative to the muon stop time $t = 0$. $\varepsilon_{\rm e}$ is the detection efficiency of muon decay electrons and the time factor

$$f_t = 1 - e^{-\lambda_{\rm He}\Delta t} \tag{12}$$

is the probability that a muon decays in the ground state of μHe during the time interval Δt.

It should be noted, that the coefficient $\varepsilon_{\rm e} f_t$ is not required as an absolute number for the determination of the intensities $I_{x-{\rm e}}^{\rm He}$ as it enters the numerator and denominator of Eq. (10) in the same manner. However, it is needed for the $D_2 + {}^3$He analysis. The quantity $\varepsilon_{\rm e} f_t$ is determined by comparing Eqs. (5) and (10) yielding

$$\varepsilon_{\rm e} f_t = \frac{N_{x-{\rm e}}^{\rm He}}{N_x^{\rm He}}\,. \tag{13}$$

Another interesting problem is the study of μHe atoms in excited metastable $2s$ states. One can expect, according to Refs. [55, 56, 57, 58], that the $(\mu{\rm He})_{2s}$ atom population varies between 5% and 7% under our experimental conditions for runs I and II. The two possible channels of $2s \to 1s$ deexcitation are two–photon transition with a rate $\lambda_{2\gamma} \sim 1.06 \times 10^5\,{\rm s}^{-1}$ [59, 60] and the Stark $2s \to 2p \to 1s$ deexcitation [55, 56, 57] induced by collisions of $(\mu{\rm He})_{2s}$ atoms with the surrounding atoms or molecules. The corresponding rate for the experimental conditions of runs I and II is $\lambda \sim 2.2 \times 10^7\,{\rm s}^{-1}$. If the time of Stark induced transitions is shorter than the resolution time of the germanium detector the corresponding $K\alpha$ transition would be experimentally classified as a prompt event. Otherwise, it would be possible to extract an upper bound for Stark induced transition rates.

B. $D_2 + {}^3$He mixtures

In a $D_2 + {}^3$He mixture one observes Kx lines arising from the deexcitation of μHe atoms formed not only due to direct muon capture by helium nuclei (as in pure helium) but also due to muon transfer from muonic deuterium to helium. Because the $d\mu$ atoms deexcitation time is of the order $10^{11}\,\mathrm{s}^{-1}$ (under our experimental conditions) the corresponding emission of K series transitions occurs practically immediately after a muon stop in the mixture and can be classified as a prompt event. Muons are captured by D_2 and ^{3}He according to the capture law [2]. Information about relative rates of atomic muon capture by deuterons and helium nuclei in a $D_2 + {}^3$He mixture as well as the probability that an excited $(d\mu)^*$ atom reaches its ground state when the muon also has the possibility of transferring directly from an excited state to a heavier nucleus, in our case helium ($\mathrm{q}_{1s}^{\mathrm{He}}$ probability) is of unquestionable importance for understanding kinetics in muon catalyzed fusion (μCF). A method for determining the characteristics of MA processes in $D_2 + {}^3$He mixture is presented in the following subsections.

1. *Muon stopping powers ratio*

A muon entering the $D_2 + {}^3$He mixture may be captured by deuterium or helium into atomic orbits of excited $d\mu$ or μHe atoms. The corresponding relative probability has the following form [21, 61, 62, 63, 64]

$$W_{\mathrm{D}} = \frac{1}{1 + A \cdot c_{\mathrm{He}}}\,, \qquad W_{\mathrm{He}} = \frac{A \cdot c_{\mathrm{He}}}{1 + A \cdot c_{\mathrm{He}}}\,, \tag{14}$$

where c_{He} is the relative atomic helium concentration in the $D_2 + {}^3$He mixture and A is the muon stopping power ratio,

$$A = \frac{(dE/dx)_{\mathrm{He}}}{(dE/dx)_{\mathrm{D}}}\,, \tag{15}$$

with $(dE/dx)_{\mathrm{He}}$ and $(dE/dx)_{\mathrm{D}}$ the ionization energy loss of muon per one atom of helium and deuterium.

The muon stopping power ratio A may be experimentally determined from the yield of electrons produced in muon decay processes in pure helium and in $D_2 + {}^3$He mixture. However, the same constant momentum of the muonic beam must be kept during expositions with both targets. The experiment relies upon the determination of a density of a pure helium target, $\tilde{\varphi}_{\mathrm{He}}$, (by variation of the target density) such that the number of muon stops in the target (and consequently the number of electrons arising from muons decaying from the $d\mu$ and ^{3}He ground state atoms) is the same as the one obtained for a given $D_2 + {}^3$He mixture. Under this condition the moderation thickness of the pure helium target is the same as the one of the $D_2 + {}^3$He mixture with density φ_{mix} and helium concentration c_{He}, given in Table I, run III. Using Eq. (14) one can determine the corresponding equivalent density of the pure helium target as

$$A \cdot \tilde{\varphi}_{\mathrm{He}} = (c_{\mathrm{D}} + A \cdot c_{\mathrm{He}})\varphi_{mix}\,, \tag{16}$$

where φ_{mix} is the atomic density of the $D_2 + {}^3$He mixture normalized to LHD and c_{D} and c_{He} are the relative deuterium and helium concentrations ($c_{\mathrm{D}} + c_{\mathrm{He}} = 1$).

Analogously, one can use a pure deuterium target instead of the helium one to determine the equivalent deuterium target density $\tilde{\varphi}_{\mathrm{D}}$. Then, equating numbers of electrons detected in runs with pure deuterium and in the $D_2 + {}^3$He target one can obtain the equivalent density, $\tilde{\varphi}_{\mathrm{D}}$, and hence the coefficient A

$$A = \frac{\tilde{\varphi}_{\mathrm{D}} - \varphi_{mix} c_{\mathrm{D}}}{\varphi_{mix} c_{\mathrm{He}}}\,. \tag{17}$$

It should be noted, however, that a determination of A from Eq. (17) with the same accuracy as from Eq. (16) requires a significantly greater helium concentration in the $D_2 + {}^3$He mixture.

2. *The $\mathrm{q}_{1s}^{\mathrm{He}}$ probability*

Prompt Lyman series transitions in μHe atoms are also observed in a $D_2 + {}^3$He mixture. As mentioned previously, they originate from direct muon capture by deexcitation of $(\mu\mathrm{He})^*$ atoms or by muon transfer from excited muonic deuterium to helium. However, the relative intensities of K series transitions measured in a $D_2 + {}^3$He mixture differ from the ones in pure helium because effective reaction rates of μHe deexcitation processes depend on the target conditions.

$\mathrm{q}_{1s}^{\mathrm{He}}$ represents the $(d\mu)^*$ atom probability to reach the ground state in a $D_2 + {}^3$He mixture and is defined as

$$\mathrm{q}_{1s}^{\mathrm{He}} = \frac{n_{d\mu}^{1s}}{n_{d\mu}^{*}}\,, \tag{18}$$

where $n_{d\mu}^{*}$ is the number of $d\mu$ atoms created in the excited state due to direct muon capture in deuterium atoms, and $n_{d\mu}^{1s}$ is the number of the $d\mu$ atoms which reach the ground state during the cascade. The number of $d\mu$ atoms created in the excited state can be written as

$$n_{d\mu}^{*} = N_{\mathrm{stop}}^{\mathrm{D/He}} \cdot W_{\mathrm{D}} \tag{19}$$

where $N_{\mathrm{stop}}^{\mathrm{D/He}}$ represents the number of muon stops in the $D_2 + {}^3$He gas mixture.

Since our setup is not able to measure $n_{d\mu}^{1s}$, we used another method to determine $\mathrm{q}_{1s}^{\mathrm{He}}$. The number of μHe atoms formed in excited states due to muon transfer from $(d\mu)^*$ to helium, $(d\mu)^* + \mathrm{He} \rightarrow (\mathrm{He}\mu)^* + d$, is $n_{\mathrm{He}\mu^*}^{\mathrm{transf}}$ and corresponds to

$$n_{\mathrm{He}\mu^*}^{\mathrm{transf}} = n_{d\mu}^{*} - n_{d\mu}^{1s}\,. \tag{20}$$

The total number of μHe atoms created in the excited states and emitting prompt Kx lines is given by the yield

$$Y_{tot}^{\mathrm{D/He}} = \sum_{x=\alpha,\beta,\gamma} \frac{N_x^{\mathrm{D/He}}}{(1-\eta_x)\varepsilon_x}\,. \tag{21}$$

On the other hand, $n^{\rm dir}_{{\rm He}\mu^*}$ is the number of μHe atoms formed in the excited states in a $\rm D_2 + {}^3He$ mixture due to direct muon capture by helium atoms

$$n^{\rm dir}_{{\rm He}\mu^*} = Y^{\rm D/He}_{tot} - n^{\rm transf}_{{\rm He}\mu^*} = N^{\rm D/He}_{\rm stop} \cdot W_{\rm He} \qquad (22)$$

Isolating $n^{1s}_{d\mu}$ in Eq. (20), using Eqs. (19) and (22), we obtain the $\mathrm{q}^{\rm He}_{1s}$ probability as

$$\mathrm{q}^{\rm He}_{1s} = (1 + A \cdot c_{\rm He}) \left[1 - \frac{Y^{\rm D/He}_{tot}}{N^{\rm D/He}_{\rm stop}} \right] . \qquad (23)$$

In the case of detecting events by the germanium detector in coincidence with muon decay electrons, the total yield $Y^{\rm D/He}_{tot}$ in Eq. (23) has to be replaced by

$$Y^{\rm D/He}_{tot,\rm e} = \frac{1}{\varepsilon_{\rm e} f_t} \sum_{x=\alpha,\beta,\gamma} \frac{N^{\rm D/He}_{x-\rm e}}{(1-\eta_x)\varepsilon_x} . \qquad (24)$$

3. *Radiative molecular peak*

The delayed muonic x rays are generated by two different mechanisms initiated by $d\mu$ atoms in their ground state. The first mechanism described in this section is simply molecular muon transfer, specifically Eq. (1a) accompanied by a 6.85 keV γ–rays. Experimental molecular muon transfer from muonic deuterium to helium $\lambda_{d^3\rm He}$ is presented in detail in many papers, in particular in Refs. [31, 38] together with the corresponding reaction rates. Below radiative decay rate of the $d\mu^3$He complex Eq. (1a) can be measured as follows.

The time distribution of the γ rays (relative to the muon stop time) falls (in a pure target) experimentally off with the disappearance rate of the muonic deuterium ground state, $\lambda_{d\mu}$,

$$\frac{dN_{6.85}}{dt} = A_{d\mu} \cdot e^{-\lambda_{d\mu} t} , \qquad (25)$$

with $A_{d\mu}$ the amplitude and

$$\begin{aligned} \lambda_{d\mu} &= \lambda_0 + \lambda_{d^3\rm He} \varphi c_{\rm He} \\ &+ \tilde{\lambda}_{dd\mu} \varphi c_{\rm D} \left[1 - W_{\rm D} \mathrm{q}^{\rm He}_{1s} (1 - \beta \omega_d) \right] . \end{aligned} \qquad (26)$$

$\lambda_{d^3\rm He}$ is the molecular formation rate for the $d\mu^3$He molecule, $\lambda_0 = 0.455 \times 10^6\,\rm s^{-1}$ is the free muon decay rate. $\tilde{\lambda}_{dd\mu}$ is the effective $dd\mu$ molecule formation rate, β the relative probability of nuclear fusion in $dd\mu$ with neutron production in the final channel and ω_d is the muon sticking probability to helium produced in nuclear $d-d$ fusion (see [38]).

The probability of the radiative decay of the $d\mu^3$He system (corresponding to the $2p\sigma \rightarrow 1s\sigma$ transition) is defined by

$$\kappa_{d\mu\rm He} = \frac{\lambda_\gamma}{\lambda_p + \lambda_\gamma + \lambda_e} . \qquad (27)$$

where λ_γ, λ_p, and λ_e are the reaction rates for the $d\mu^3$He molecular decay according to channels (a), (b) and (c) of Eq. (1), respectively, also shown in Fig. 2. The formation of the $d\mu^3$He molecule practically coincides with the subsequent γ–ray emission because of the very short average life–time of $d\mu^3$He molecule ($\sim 10^{11}\,\rm s^{-1}$ [2, 20, 22, 28, 29]).

In the present experiment only the radiative decay channel is detected. The corresponding $\kappa_{d\mu\rm He}$ probability is determined by the ratio

$$\kappa_{d\mu\rm He} = \frac{N^{d\mu^3\rm He}_\gamma}{N^{d\mu^3\rm He}_{tot}} , \qquad (28)$$

where $N^{d\mu^3\rm He}_{tot}$ and $N^{d\mu^3\rm He}_\gamma$ are the total number of $d\mu^3$He molecules formed in the mixture and the number of molecules subsequently decaying via the radiative channel, Eq. (1a), respectively). The latter quantity may be expressed as

$$N^{d\mu^3\rm He}_\gamma = \frac{N_{6.85}}{\varepsilon_{6.85} F_t (1 - \eta_{6.85})} , \qquad (29)$$

where $N_{6.85}$ is the number of 6.85 keV γ-rays during time Δt_γ elapsed after a muon stop and $\varepsilon_{6.85}$ is the corresponding detection efficiency. The factor F_t

$$F_t = e^{-\lambda_{d\mu} t} (1 - e^{-\lambda_{d\mu} \Delta t_\gamma}) \qquad (30)$$

is the γ–ray detection time factor and $\eta_{6.85}$ is the 6.85 keV γ–ray attenuation coefficient. For the γ rays detected with the del-e criterion, a corresponding $N^{d\mu^3\rm He}_\gamma$ value is obtained using Eq. (29) divided by the $\varepsilon_{\rm e} f_t$ coefficients.

A comparison of the $N^{d\mu^3\rm He}_\gamma$ value measured with and without del-e criterion provides also a test for the validity of our coefficients $\varepsilon_{\rm e}$, f_t, and $N_{6.85}$. The detection efficiency $\varepsilon_{6.85}$ was determined by MC simulations including feasible space distributions of muon stops in the target volume and experimental detection efficiencies of Kx lines for the pure ^{3}He runs.

The total number of the $d\mu^3$He molecules formed in $\rm D_2 + He$ mixture is determined by analyzing the 6.85 keV γ–ray time distribution. It is expressed as

$$N^{d\mu^3\rm He}_{tot} = \frac{\lambda_{d^3\rm He} \varphi c_{\rm He}}{\lambda_{d\mu}} n^{1s}_{d\mu} , \qquad (31)$$

where $n^{1s}_{d\mu}$ is the number of $d\mu$ atoms formed via direct muon capture and reached the ground state after deexcitation. By measuring the exponential time distribution (25) and using the known quantities λ_0, $\tilde{\lambda}_{dd\mu}$, $W_{\rm D}$, ω_d, $\mathrm{q}^{\rm He}_{1s}$, β [65, 66, 67] one can determine the molecular formation rate $\lambda_{d^3\rm He}$ from Eq. (26). The determination of $N^{tot}_{d\mu^3\rm He}$ from Eq. (31) requires in addition the knowledge of $n^{1s}_{d\mu}$, isolated in Eqs. (18) and (19). By substituting $N^{d\mu^3\rm He}_\gamma$ and $N^{d\mu^3\rm He}_{tot}$ into Eq. (28) one finally obtains the $\kappa_{d\mu\rm He}$ probability.

4. Delayed K series transitions from muonic helium

As already said, the delayed muonic x rays are generated by two different mechanisms initiated by the ground state $d\mu$ atoms. The second one discussed here is proceeded by $dd\mu$ formation (in collision of $(d\mu)_{1s}$ with D_2 molecule) and subsequently by nuclear $d-d$ fusion. Muons freed after fusion form excited muonic helium atoms due to direct muon capture by helium or due to muon capture by deuterium and subsequent muon transfer to helium. Then the delayed x rays of muonic helium K series transitions are observed.

The time distribution is also determined by $\lambda_{d\mu}$. Besides, the relative intensities $I_{x,del}$ (or $I_{x-e,del}$) of the delayed K series transitions are assumed to be the same as those of the prompt radiation of Kx lines. It is worthwhile to note that the measurement of the corresponding absolute intensities enabled us to determine the third component of $\lambda_{d\mu}$ in Eq. (26) and, consequently, to extract the effective formation rate of the $dd\mu$ molecule in the $D_2+{}^3He$ mixture using the coefficients W_{D}, q_{1s}^{He} (also obtained in this paper) and average values for β, and ω_d (taken from Refs. [65, 66, 67]).

IV. ANALYSIS

A. Relative intensities of K series transitions

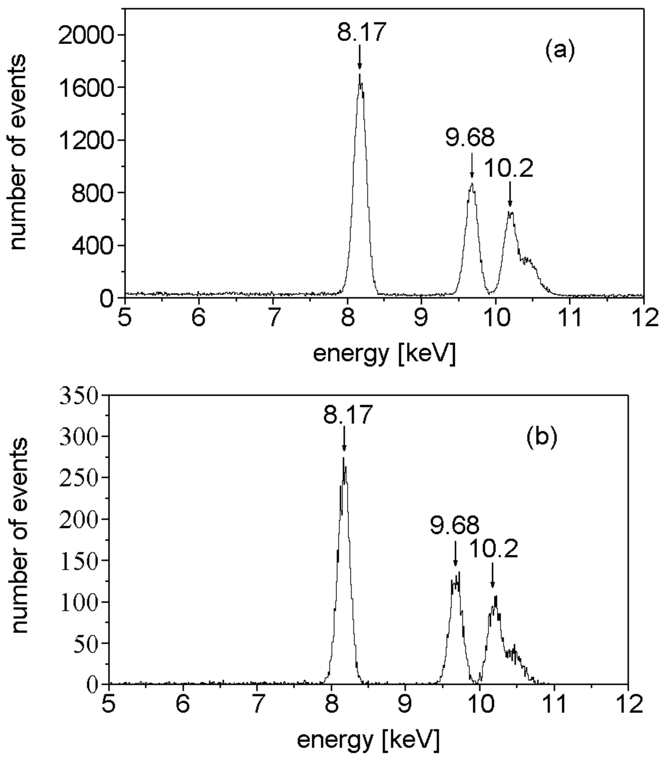

FIG. 3: Prompt events energy distribution in run I without (a) and with coincidences with muon decay electrons (b).

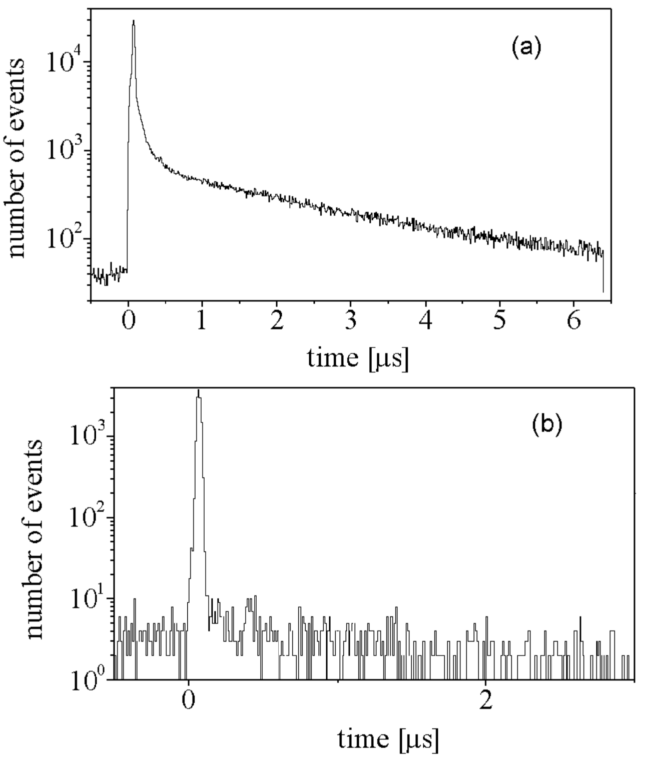

FIG. 4: Time distribution in run I without (a) and with coincidences with muon decay electrons (b).

To obtain the relative intensities of muonic x–ray K series transitions of μ^3He and μ^4He atoms in helium targets we analyzed the corresponding energy and time distributions detected by the germanium detector in runs I and II. Figures 3 and 4 present the energy and time distributions obtained in runs I with and without muon decay electrons coincidences. As seen, the del-e criterion significantly suppresses the background level and improved the signal–to–background ratio. As already mentioned before, events detected within a time interval $t_\gamma = [(-0.03)-(+0.03)]\,\mu$s relative to muon stops were classified as prompt ones. The prompt Kx lines events N_x^{He}, $N_{x-\mathrm{e}}^{\mathrm{He}}$ were determined by fitting the experimental amplitude distributions by a Gaussian distribution

$$\frac{dN_x^{\mathrm{He}}}{d\mathrm{E}_x} = A_x \cdot \exp\left[-\frac{(\mathrm{E}_x-\overline{\mathrm{E}}_x)^2}{2\sigma_x^2}\right] + S\cdot \mathrm{E}_x + O\,, \quad (32)$$

where $\overline{\mathrm{E}}_x$ is the mean value of the corresponding Kx line energy, σ_x the standard deviation for the Kx line and A_x the normalization constant. The germanium detector background is taken into account by a straight line, with S and O being the constants. Results obtained in measurements I and II are presented in Tables II and III. Statistical errors are quoted in parentheses throughout the whole text.

The analysis performed for both mixtures is similar. The prompt intensities are measured within the same time interval as for the pure helium runs, both with and without the delayed electron coincidence condition. The

TABLE II: Prompt x–ray yields of $\mu^{3,4}$He K series transitions measured in different runs with pure ^{3}He and ^{4}He.

	$K\alpha$		$K\beta$		$K\gamma$			Yield	
Range [keV]	[7.83 – 8.53]		[9.43 – 9.96]		[9.98 – 10.6]		[10^8]	[10^8]	[10^8]
Runs	N_{α}^{He}	$N_{\alpha-\mathrm{e}}^{\mathrm{He}}$	N_{β}^{He}	$N_{\beta-\mathrm{e}}^{\mathrm{He}}$	N_{γ}^{He}	$N_{\gamma-\mathrm{e}}^{\mathrm{He}}$	Y_{α}^{He}	Y_{β}^{He}	Y_{γ}^{He}
I (^{3}He)	34 319(190)	4785(70)	17 835(139)	2551(52)	20 045(150)	2834(54)	7.536(90)	3.795(53)	4.231(62)
IIa (^{4}He)	7295(87)	985(32)	4919(72)	688(26)	2616(55)	408(20)	0.897(14)	0.585(10)	0.309(8)
IIb (^{4}He)	11 587(111)	1593(40)	7547(91)	1009(32)	4627(76)	613(25)	1.766(25)	1.126(18)	0.677(13)
IIc (^{4}He)	1303(38)	174(14)	709(29)	91(10)	846(33)	123(12)	0.287(9)	0.151(6)	0.178(7)

TABLE III: Relative intensities of prompt x rays of $\mu^{3,4}$He K series transitions measured in runs with pure helium. For each run, results from both the full statistics and the del-e condition are given.

	I_{α}^{He} [%]	$I_{\alpha-\mathrm{e}}^{\mathrm{He}}$ [%]	I_{β}^{He} [%]	$I_{\beta-\mathrm{e}}^{\mathrm{He}}$ [%]	I_{γ}^{He} [%]	$I_{\gamma-\mathrm{e}}^{\mathrm{He}}$ [%]
I (^{3}He)	48.4(8)	47.8(9)	24.4(4)	24.8(6)	27.2(4)	27.4(6)
IIa (^{4}He)	50.0(9)	47.3(19)	32.7(7)	33.1(14)	17.3(5)	19.6(13)
IIb (^{4}He)	49.5(9)	49.5(15)	31.5(6)	31.4(11)	19.0(5)	19.1(8)
IIc (^{4}He)	46.6(18)	44.8(44)	24.5(11)	23.5(29)	28.9(13)	31.7(35)
Augsburger *et al.* [20] (^{4}He)	46.9(45)	—	27.9(28)	—	25.2(19)	—
Tresch *et al.* [22][a]	47.0(2)	—	20.3(10)	—	32.7(16)	—

[a] for ^{3}He ($\varphi = 0.026$) and for ^{4}He ($\varphi = 0.0395$)

results, given in Table V, depend on the pressure of the $D_2 + {}^3$He mixture. For comparison, results of Augsburger *et al.* [20] taken at a similar pressure as in run III, are also shown in the table. The differences in relative intensity between pure helium and the deuterium–helium mixtures are essentially due to excited state transfer. Additionally, such an analysis allows us to determine the Kx transition energy differences between the two helium isotopes. The $\Delta E(^4\mathrm{He} - {}^3\mathrm{He})$ energy differences are given in Table IV. A theoretical prediction exists for the $K\alpha$ transition [68] which is slightly lower than our measured value.

TABLE IV: Kx transition energy differences between the two helium isotopes. The last column gives a theoretical prediction for the $K\alpha$ transition.

Transitions	$\Delta E(^4\mathrm{He} - {}^3\mathrm{He})$ [eV]		
	Our work	Tresch *et al.* [22]	Rinker [68]
$K\alpha$	77.8 ± 0.9	75.0 ± 1.0	74.2
$K\beta$	92.9 ± 1.1	—	
$K\gamma$	103.4 ± 3.4	—	

B. Stopping power ratio measurement

The stopping power ratio A was determined by analyzing the time spectra of muon decay electrons measured by the scintillator pairs in the runs with pure helium (run I) and the $D_2 + {}^3$He mixture (run III). Measurements with pure helium were performed to find a corresponding equivalent density $\tilde{\varphi}_{\mathrm{He}}$ (see Eq. (16) resulting in the same number of muon stops in the target volume as the one in the $D_2 + {}^3$He mixture (run III). Variation of the helium target density enabled us to find a density dependence of muon stops and hence $\tilde{\varphi}_{\mathrm{He}}$. The A stopping power ratio was the determined according to Eq. (16). Note that the linear density dependence of muon stops in gases is a good approximation, if the gaseous mixture thickness expressed in terms of energy is significantly greater than the energy dispersion of the muon beam. This condition is fulfilled in our experiments.

Due to muons stopping also in aluminum and gold (target walls) besides in the gas, the electron time spectra are a sum of exponential functions:

$$\begin{aligned} \frac{dN_e}{dt} &= A^e_{\mathrm{Al}} \cdot e^{-\lambda_{\mathrm{Al}} \cdot t} + A^e_{\mathrm{Au}} \cdot e^{-\lambda_{\mathrm{Au}} \cdot t} \\ &+ A^e_{\mathrm{He}} \cdot e^{-\lambda_{\mathrm{He}} \cdot t} + B^e, \end{aligned} \tag{33}$$

where A^e_{Al}, A^e_{Au}, and A^e_{He} are the corresponding normalization amplitudes and

$$\begin{aligned} \lambda_{\mathrm{Al}} &= Q_{\mathrm{Al}} \cdot \lambda_0 + \lambda^{\mathrm{Al}}_{\mathrm{cap}} \\ \lambda_{\mathrm{Au}} &= Q_{\mathrm{Au}} \cdot \lambda_0 + \lambda^{\mathrm{Au}}_{\mathrm{cap}} \\ \lambda_{\mathrm{He}} &= \lambda_0 + \lambda^{\mathrm{He}}_{\mathrm{cap}}, \end{aligned} \tag{34}$$

are the muon disappearance rates in the different elements (the rates are the inverse of the muon lifetimes in the target wall materials). The nuclear capture rates in aluminum and gold, $\lambda^{\mathrm{Al}}_{\mathrm{cap}} = 0.7054(13) \times 10^6\ \mathrm{s}^{-1}$ and

TABLE V: Relative intensities, in percent, of prompt x rays of μ^3He K series transitions measured in runs III and IV. "Full" stands for full statistics, whereas del-e represents the delayed electron criterion. The last column presents the results of Augsburger *et al.* [20].

Runs	III		IV		Augsburger *et al.* [20]
Transitions	full	del-e	full	del-e	
$I_\alpha^{\mathrm{D/He}}$	66.4(7)	65.7(15)	72.0(6)	72.9(16)	68.6(51)
$I_\beta^{\mathrm{D/He}}$	26.6(5)	26.5(8)	24.5(3)	24.1(8)	24.5(19)
$I_\gamma^{\mathrm{D/He}}$	7.0(4)	7.8(4)	3.5(1)	3.0(3)	6.9(6)

$\lambda_{\mathrm{cap}}^{\mathrm{Au}} = 13.07(28) \times 10^6$ s^{-1}, are known [54]. Q_{Al} and Q_{Au} are the Huff factors, which take into account that muons are bound in the 1s state of the respective nuclei when they decay. This factor is negligible for helium but necessary for aluminum $Q_{\mathrm{Al}} = 0.993$ and important for gold $Q_{\mathrm{Au}} = 0.850$ [54]. The constant B^e characterizes the random coincidence background.

By measuring the helium amplitude, A^e_{He},

$$A^e_{\mathrm{He}} = N^{\mathrm{He}}_{\mathrm{stop}} \cdot \varepsilon_e \cdot \lambda_0 \qquad (35)$$

and knowing the electron detection efficiencies averaged over the energy distributions (ε_e), one obtains the number of muons stopping in helium $N^{\mathrm{He}}_{\mathrm{stop}}$.

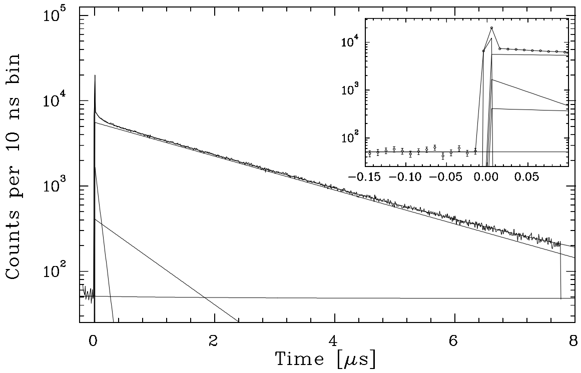

FIG. 5: Time distribution of muon-decay electrons measured in run I. The inset shows details at early times.

Figure 5 shows the time distribution of the muon decay electrons measured in run I with the three exponential fit (Eq. (33)). The ratio R of muons stopped in the target, i.e., the number of detected electrons N_e, divided by the number of muons entering the target N_μ

$$R(\varphi) = \frac{N_e}{N_\mu} = a\varphi + b \qquad (36)$$

depends on the helium density. Table VI shows the measured values of R in percent for each measurements. By fitting R as a function of φ, one obtains

$$a = -(0.60 \pm 0.11) \qquad b = (0.099 \pm 0.005) \qquad (37)$$

The value of $\tilde{\varphi}_{\mathrm{He}}$ was determined from the condition

$$R(\tilde{\varphi}_{\mathrm{He}}) = R(\mathrm{D/He})\,, \qquad (38)$$

where $R(\tilde{\varphi}_{\mathrm{He}})$ and $R(\mathrm{D/He})$ are the ratios for pure ^{3}He (at the density $\tilde{\varphi}_{\mathrm{He}}$) and for the D$_2$ + ^{3}He mixture, respectively. We found

$$\tilde{\varphi}_{\mathrm{He}} = 0.0361 \left[{}^{+0.0084}_{-0.0057}\right] . \qquad (39)$$

The corresponding value of A, using Eq. (16), is then

$$A = 1.67 \left[{}^{+0.35}_{-0.33}\right] . \qquad (40)$$

TABLE VI: R ratio measurements for runs I and run III. N_μ is the number of muons entering the target and N_e the number of detected electrons. The beam momentum was p_μ = 34.0 MeV/c.

Run	N_μ [10^6]	N_e [10^6]	R [10^{-2}]	φ [LHD]
Ia	1362.5	103.8(4)	7.62(3)	0.0363
Ib	704.3	54.3(3)	7.72(4)	0.0359
Ic	750.7	58.2(3)	7.75(4)	0.0355
Id	413.6	32.5(2)	7.85(6)	0.0337
III	8875.2	683.6(11)	7.70(1)	0.0585

The muon stopping power ratio A of helium to deuterium atoms coincides (within the experimental errors) with the results of Refs. [21, 69] obtained under quite different experimental conditions. Our rather large relative errors, ≈ 20%, are a consequence of small statistics and the relatively small range of variations of ^{3}He and D$_2$ + ^{3}He target densities.

C. $\mathrm{q}^{\mathrm{He}}_{1s}$ probability

On of the main aim of runs III and IV was a measurement of the $\mathrm{q}^{\mathrm{He}}_{1s}$ probability. In order to determine this quantity it was necessary to know (according to Eqs. (18)-(23)) the muon stopping power ratio A, the prompt K series transition yields of μ^3He atoms in pure ^{3}He and in D$_2$ + ^{3}He mixtures, N_x^{He} and $N_x^{\mathrm{D/He}}$, and the numbers of muon stops in pure ^{3}He and in D$_2$ + ^{3}He mixtures, N_{stop}. Significant background reduction was achieved by using the del-e criterion. The results are presented in Table VII. Note the excellent agreement between full statistics and del-e analysis.

TABLE VII: Experimental values of $\mathrm{q}_{1s}^{\mathrm{He}}$ obtained from the $\mathrm{D}_2 + {}^3\mathrm{He}$ experiments. "Full" stands for the full statistics, whereas del-e represent the delayed electron criterion.

Runs	Statistics	$\sum\limits_{x=\alpha,\beta,\gamma} N_x^{\mathrm{D/He}}$	$Y_{tot}^{\mathrm{D/He}}$ [10^8]	$\mathrm{q}_{1s}^{\mathrm{He}}$
III	full	35 376(270)	7.70(15)	0.882(18)
	del-e	4968(72)	7.60(29)	0.885(21)
IV	full	37 402(205)	5.71(11)	0.844(20)
	del-e	5161(75)	5.85(23)	0.838(23)

Figure 6 shows the energy dependence of the theoretical $\mathrm{q}_{1s}^{\mathrm{He}}$ values versus $d\mu + {}^3\mathrm{He}$ collision energy calculated for runs III and IV in the framework of the simple $(d\mu)^*$ cascade model [16, 17, 70] and compares then with experiment. The model assumes that the kinetic energy of $(d\mu)^*$ atoms remains unchanged during deexcitation. The $\mathrm{q}_{1s}^{\mathrm{He}}$ value is determined from deexcitation and muon transfer to helium. A complicated interplay between these two processes is described by a system of linear first order differential equations for level populations, $N_{nl}(t)$, with $n \leq 12$. The $\mathrm{q}_{1s}^{\mathrm{He}}$ is defined as

$$\mathrm{q}_{1s} = N_{1s}(t \rightarrow \infty)\,. \tag{41}$$

The deexcitation scheme is taken from Ref. [17] and the corresponding reaction rates are collected in Refs. [16, 17].

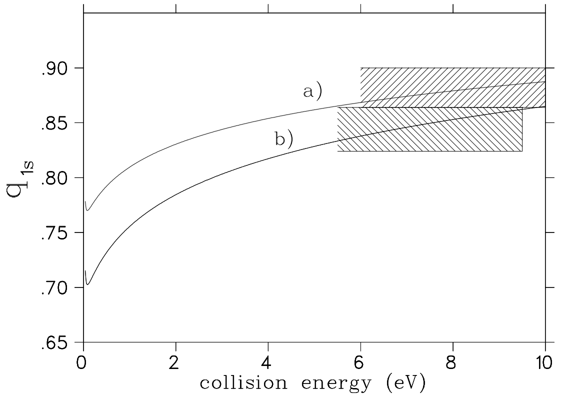

FIG. 6: Energy dependence of theoretical $\mathrm{q}_{1s}^{\mathrm{He}}$ in $\mathrm{D}_2 + {}^3\mathrm{He}$ mixture calculated for runs III (curve a) and IV (curve b). Experimental values of the $\mathrm{q}_{1s}^{\mathrm{He}}$ measured in the present work ($\mathrm{q}_{1s}^{\mathrm{He}} = (0.882 \pm 0.018)$ and $\mathrm{q}_{1s}^{\mathrm{He}} = (0.844 \pm 0.020)$) are represented by hatched boxes defined by their values and errors.

As seen from Fig. 6, the experimental values of $\mathrm{q}_{1s}^{\mathrm{He}}$ coincide with the theoretical ones for an average $d\mu$–He collision energy around 8 eV. Note the pronounce difference between the experimental values of $\mathrm{q}_{1s}^{\mathrm{He}}$ and the theoretical ones corresponding to fully thermalized $d\mu$ atoms. However, more refined theoretical calculations of $\mathrm{q}_{1s}^{\mathrm{He}}$ based on Monte Carlo simulations of acceleration of $d\mu$ atoms due to deexcitation processes and muon transfer to helium as well as thermalisation due to elastic collisions are required to arrive at definite conclusions. It should also be noted that experimental results presented in this paper agree with earlier ones (see Ref. [71]). On the other hand, analogous comparison with results presented in Refs. [20, 21, 22, 61] is not possible due to significantly different helium concentrations and densities.

D. Radiative branching ratio $\kappa_{d\mu\mathrm{He}}$

The experimental method to determine the $d\mu{}^3\mathrm{He}$ radiative decay branching ratio $\kappa_{d\mu\mathrm{He}}$ is described in Sec. III B 3. Energy and time distributions of prompt and delayed events detected in runs III and IV with muon decay electron coincidences are presented in Figs. 7 to 9.

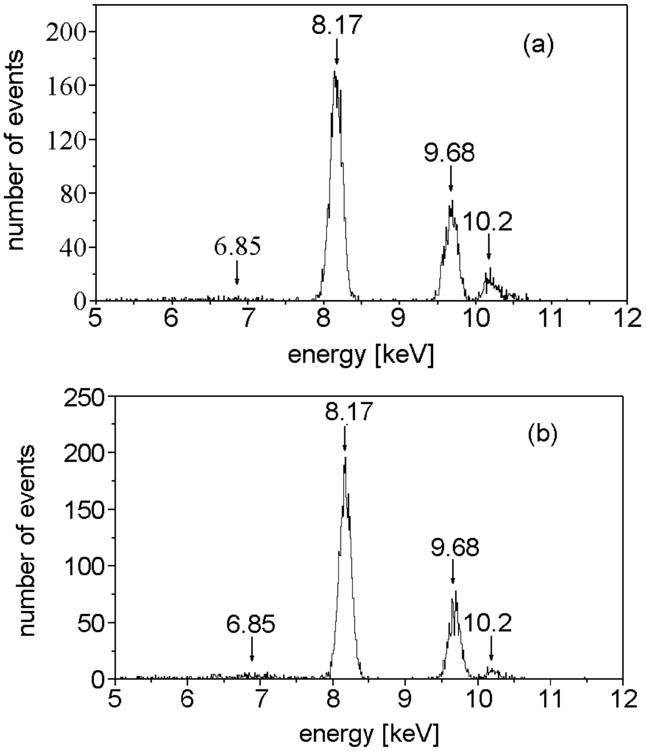

FIG. 7: Energy spectra of the prompt event with the del-e criterion in runs III and IV.

To determine the $\lambda_{d\mu}$ and $\lambda_{d^3\mathrm{He}}$ rates (see Eq. (26)) the γ–ray time distributions were fitted within the energy range [5.74 – 7.50] keV using the expression

$$\begin{aligned}\frac{dN_{6.85}}{dt} &= A_{d\mu}^{\gamma}\cdot e^{-\lambda_{d\mu}t} + A_{\mathrm{Au}}^{\gamma}\cdot e^{-\lambda_{\mathrm{Au}}t} + A_{\mathrm{Al}}^{\gamma}\cdot e^{-\lambda_{\mathrm{Al}}t}\\ &+ D^{\gamma}\cdot e^{-\lambda_0 t} + F^{\gamma}\,,\end{aligned} \tag{42}$$

where $A_{d\mu}^{\gamma}$, A_{Au}^{γ}, and A_{Al}^{γ} are the normalization constants of the different target elements. D^{γ} and F^{γ} are the constants describing the germanium background.

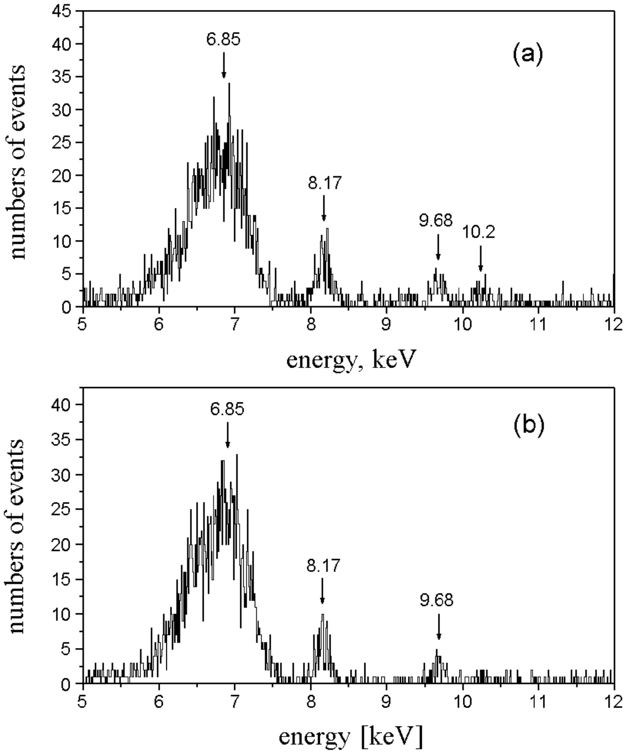

FIG. 8: Energy spectra of the delayed event with the del-e criterion in runs III and IV.

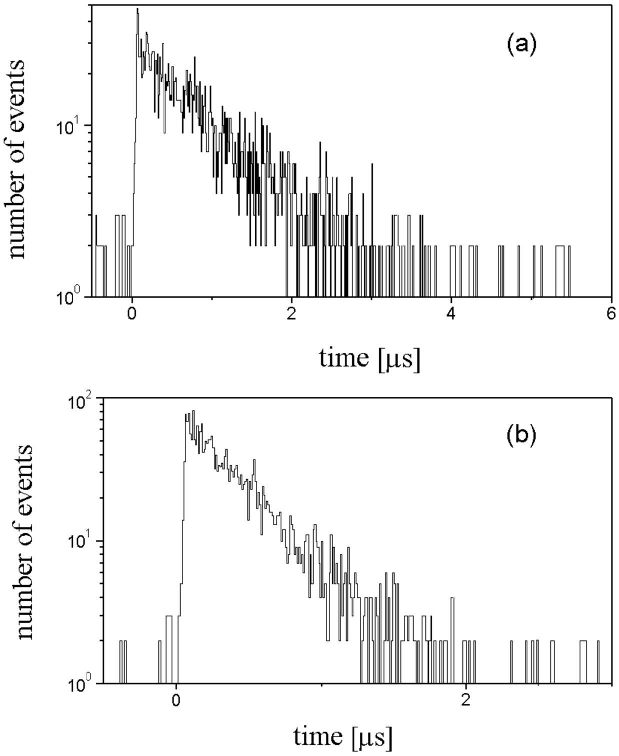

FIG. 9: Delayed event time distributions with the del-e criterion in runs III and IV within the energy range [5.74 − 7.50] keV.

TABLE VIII: Experimental results for the muonic deuterium ground state disappearance rate and the $d\mu^3$He molecular formation rate.

Runs	$\lambda_{d\mu}$ [μs^{-1}]	$\lambda_{d^3\mathrm{He}}$ [μs^{-1}]
III	$1.152(36)_{stat}(30)_{syst}$	$240(13)_{stat}(15)_{syst}$
IV	$2.496(58)_{stat}(100)_{syst}$	$244(6)_{stat}(16)_{syst}$
Average		242(20)
Maev *et al.* [72]		232(9), 233(16)^a
Gartner *et al.* [28]		185.6(77)

^{a}at 50 K and 39.5 K, respectively

The results of runs III and IV for the muonic deuterium ground state disappearance rate and the molecular formation rate $\lambda_{d^3\mathrm{He}}$, using Eq. (26), are shown in Table VIII. The averaged value $\lambda_{d^3\mathrm{He}} = 242(20)$ $\mu\mathrm{s}^{-1}$, where the errors include statistical as well as systematic errors is consistent with the measurement of Maev *et al.* [72], but is in disagreement with the work of Gartner *et al.* [28].

According to Eq. (28) the determination of the branching ratio $\kappa_{d\mu\mathrm{He}}$ requires the knowledge of both the total number of $d\mu^3$He molecules formed in a mixture and the number of $d\mu^3$He's decaying via the radiative channel, Eq. (1a). The corresponding numbers $N_{tot}^{d\mu^3\mathrm{He}}$ and $N_{\gamma}^{d\mu^3\mathrm{He}}$ were determined using Eqs. (29) and (31). The γ rays were measured during a time t_γ and the del-e time interval was $t_e - t_\gamma$. The $\varepsilon_{6.85}$ detection efficiency was determined using detection efficiencies of μ^3He atom K series transitions in runs I and II by a MC simulation. This MC calculation took into account the $\eta_{6.85}$ attenuation of γ rays passing through all layers between the germanium detector and the gas. The time factors f_t for the electrons and F_t for the γ rays are slightly different for both runs, $f_t = 0.84$ and $F_t = 0.94$ for run III, and $f_t = 0.86$ and $F_t = 0.99$ for run IV. All results are presented in Table IX.

The $\kappa_{d\mu\mathrm{He}}$ values obtained in the present experiment for two different D$_2$ + ^{3}He densities differ somewhat from the experimental result of Ref. [20], i.e., $\kappa_{d\mu\mathrm{He}} = (0.301 \pm 0.061)$ performed under slightly different experimental conditions ($\varphi = 0.697$, $c_{\mathrm{He}} = 0.0913$). Our results differ slightly from the calculated $\kappa_{d\mu\mathrm{He}}$ value in Ref. [30] for a total angular momentum $J = 0$ of the $d\mu^3$He complex. However, they are in a good agreement with the calculations of Refs. [29, 73] for a total angular momentum $J = 1$.

A close comparison of the existing theoretical results for $\kappa_{d\mu\mathrm{He}}$, [27, 29, 30, 73, 74, 75], with their experimental results obtained in the present paper and in Ref. [20] may throw some light on the mechanism of rotational $J = 1 \rightarrow J = 0$ transitions of $d\mu^3$He molecules in the $2p\sigma$ state, labeled $\tilde{\lambda}_{10}$ in Fig. 2. Specifically, two different mechanism of the $J = 1 \rightarrow J = 0$ transition were

TABLE IX: Experimental results concerning formation and decay processes of $d\mu^3$He molecules obtained from runs III and IV. "Full" stands for the full statistics, whereas del-e represents the delayed electron criterion. The 6.85 keV γ rays were measured within an energy range [5.74 − 7.55] keV. The time intervals for the γ rays and electrons are also given.

Parameter	Units	Run III		Run IV	
		full	del-e	full	del-e
t_γ	[μs]	[(−0.03) − (+2.5)]	[(−0.03) − (+2.5)]	[(−0.03) − (+1.8)]	[(−0.03) − (+1.8)]
$t_e - t_\gamma$	[μs]	–	[0.08 − 4.6]	–	[0.08 − 4.9]
$N_{6.85}$	[10^3]	17.42(21)	2.15(6)	20.07(23)	2.63(7)
$N_{tot}^{d\mu^3\mathrm{He}}$	[10^3]	20.81(136)	20.86(136)	16.50(70)	16.41(72)
$N_\gamma^{d\mu^3\mathrm{He}}$	[10^3]	4.20(10)	4.37(17)	3.76(10)	3.53(18)
$\varepsilon_{6.85}(1-\eta_{6.85})$	[10^{-5}]	4.15(8)	5.76(15)	6.26(19)	8.72(32)
$\kappa_{d\mu\mathrm{He}}$		0.203(14)	0.209(17)	0.228(12)	0.213(15)

proposed in Refs. [31, 32, 33] and [34]. Both mechanisms start with an Auger transition in a $d\mu + {}^3$He collision,

$$d\mu + {}^3\mathrm{He} \to \left[(d\mu^3\mathrm{He})^{++}_{2p\sigma,J=1}e\right]^+ + e\,. \tag{43}$$

The first mechanism [31, 32, 33] consists of a two stage process, namely the formation of a neutral complex in the collision

$$\begin{aligned}&\left[(d\mu^3\mathrm{He})^{++}_{2p\sigma,J=1}e\right]^+ \;+\; \mathrm{He} \quad \xrightarrow{\lambda_n} \\ &\left[(d\mu^3\mathrm{He})^{++}_{2p\sigma,J=1}2e\right] \;+\; \mathrm{He}^+\,,\end{aligned} \tag{44}$$

followed by a subsequent deexcitation due to external Auger effect

$$\begin{aligned}&\left[(d\mu^3\mathrm{He})^{++}_{2p\sigma,J=1}2e\right] \;+\; \mathrm{D(D_2)} \quad \xrightarrow{\lambda^{ext}_{Aug}} \\ &\left[(d\mu^3\mathrm{He})^{++}_{2p\sigma,J=0}2e\right] \;+\; \mathrm{D^+(D_2^+)} + e\,.\end{aligned} \tag{45}$$

In the second mechanism [34], the $J = 1 \to J = 0$ transition involves a number of molecular processes. However, the corresponding transition rate is essentially determined by a molecular cluster formation

$$\begin{aligned}&\left[(d\mu^3\mathrm{He})^{++}_{2p\sigma,J=1}e\right]^+ \;+\; \mathrm{D_2} \quad \xrightarrow{\lambda_{cl}} \\ &\left[(d\mu^3\mathrm{He})^{++}_{2p\sigma,J=0}e\right]\mathrm{D_2}\end{aligned} \tag{46}$$

and a subsequent inner electron conversion

$$\begin{aligned}&\left[(d\mu^3\mathrm{He})^{++}_{2p\sigma,J=1}e\right]\mathrm{D_2} \quad \xrightarrow{\lambda^{int}_{Aug}} \\ &\left[(d\mu^3\mathrm{He})^{++}_{2p\sigma,J=0}e\right]\mathrm{D_2^+} \;+\; e\,.\end{aligned} \tag{47}$$

The first mechanism yields an effective $J = 1 \to J = 0$ transition rate

$$\tilde{\lambda}_{10} = \frac{\lambda_n \lambda^{ext}_{Aug}\varphi^2 c_\mathrm{D} c_\mathrm{He}}{\lambda^1_{dec} + \lambda^{ext}_{Aug}\varphi c_\mathrm{D} + \lambda_n \varphi c_\mathrm{He}}\,, \tag{48}$$

the second mechanism gives

$$\tilde{\lambda}_{10} = \frac{\lambda_{cl}\lambda^{int}_{Aug}\varphi^2 c_\mathrm{D}}{\lambda^1_{dec} + \lambda^{int}_{Aug} + \lambda_{cl}\varphi c_\mathrm{D}} \tag{49}$$

(see Refs. [43, 44]). The effective $d\mu^3$He decay rates are defined as

$$\lambda^J_{dec} = \lambda^J_\gamma + \lambda^J_e + \lambda^J_p\,, \tag{50}$$

for both rotational states, $J = 0$ and $J = 1$.

Because the effective transition rate $\tilde{\lambda}_{10}$ is model dependent, the ratio $\tilde{\lambda}_{10}/\lambda^1_{dec}$ may allow us to check the validity of both models. A proposal for a corresponding experiment was presented in Refs. [43, 44]. It exploits the J–dependence of the probability for the radiative $d\mu^3$He decay ratio $\kappa_{d\mu\mathrm{He}}$. An unequivocal identification of the $J = 1 \to J = 0$ transition mechanism should be possible by measuring the 6.85 keV γ–ray yields for a series of different densities of $\mathrm{D_2} + {}^3$He mixtures. The density dependence of $\kappa_{d\mu\mathrm{He}}$ normalized to a single $d\mu^3$He molecule

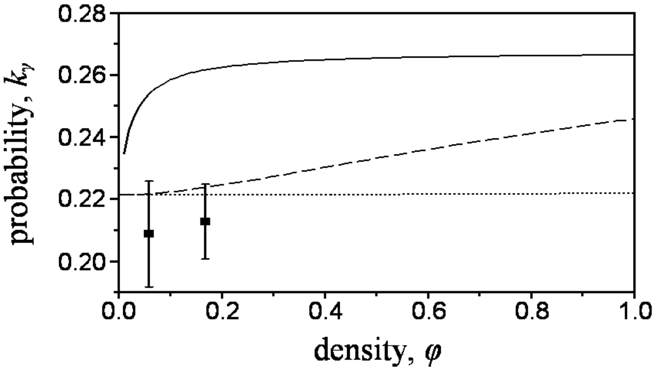

FIG. 10: Density dependence of the γ–decay branching ratio $\kappa_{d\mu\mathrm{He}}$. Points with error bars are our experimental values. The solid line corresponds to the second mechanism with $\lambda^{int}_\mathrm{Aug} = 10^{12}\,\mathrm{s}^{-1}$ [34]. The dashed lines represents the first mechanism with $\lambda^{ext}_\mathrm{Aug} = 8.5 \times 10^{11}\,\mathrm{s}^{-1}$ [31], whereas the dotted lines is given for $\lambda^{ext}_\mathrm{Aug} = 10^{10}\,\mathrm{s}^{-1}$ [32, 33].

is

$$\kappa_{d\mu\mathrm{He}} = \frac{1}{\lambda^1_{dec} + \tilde{\lambda}_{10}} \left[\lambda^1_\gamma + \frac{\tilde{\lambda}_{10}\lambda^0_\gamma}{\lambda^0_{dec}} \right] . \qquad (51)$$

Here, the decay rates $\lambda^0_{dec} = 6 \times 10^{11}$ s^{-1}, $\lambda^0_\gamma = 1.8 \times 10^{11}$ s^{-1} [30], $\lambda^1_{dec} = 7 \times 10^{11}$ s^{-1}, and $\lambda^1_\gamma = 1.55 \times 10^{11}$ s^{-1} (obtained by averaging the corresponding results taken from Refs. [27, 29, 30, 73, 74, 75, 76, 77, 78]) are model independent. Concerning the first mechanism, we used $\lambda_n = 2 \times 10^{13}$ s^{-1}, $\lambda^{ext}_{Aug} = 8.5 \times 10^{11}$ s^{-1} [31], and $\lambda^{ext}_{Aug} = 10^{10}$ s^{-1} [32, 33]. For the second mechanism, we used $\lambda_{cl} = 3 \times 10^{13}$ s^{-1} and $\lambda^{int}_{Aug} = 10^{12}$ s^{-1} [34]. All density dependent rates are normalized to LHD.

As can be seen from Fig. 10, our experimental values of $\kappa_{d\mu\mathrm{He}}$ are in better agreement with the theoretical results corresponding to the first mechanism as described in Czapliński *et al.* [31, 32, 33]. More refined calculations of the $J = 1 \rightarrow J = 0$ transition including realistic $(\mathrm{D} - d\mu^3\mathrm{He})^{0,(+\text{ or }2+)}$ interaction potentials have however to be performed before definite conclusions can be drawn. Calculations in Refs. [32, 33] go in this sense but withing the framework of a semi–classical treatment. Such a treatment seems rather problematic considering the collision energies in such a system. More accurate, i.e., purely quantum calculations are now in progress.

E. Delayed K series transitions of μHe atoms

The relative intensities $I_{del,x}$ and $I_{del,x-\mathrm{e}}$ of delayed μHe K series transitions were determined by measuring the $N_{del,x}$ events during a time interval t_γ after the muon stop (see Table X). The corresponding relative intensities were obtained from the ratios

$$I_{del,x} = \frac{N_{del,x}}{[(1-\eta_x)\varepsilon_{x\alpha}]} \Bigg/ \sum_{x=\alpha,\beta,\gamma} \frac{N_{del,x}}{[(1-\eta_x)\varepsilon_{x\alpha}]} . \qquad (52)$$

Our results should, in principle, coincide with the prompt intensities of K series transitions if we assume that the incoming muon energy distribution as well as the primary μHe atom excited states distribution due to direct muon capture are the same as the corresponding ones for muons freed after the $d-d$ fusion. The observed prompt relative intensities of the corresponding K series transitions (see Table III) are however somewhat different from the delayed ones indicating that the above conditions are probably not fulfilled.

TABLE X: Delayed muonic x–ray relative intensities for ^{3}He and ^{4}He atoms.

Run	Units	III (^{3}He)	IV (^{4}He)
t_γ	[μs]	[0.1 − 2.5]	[0.1 − 1.8]
$t_e - t_\gamma$	[μs]	[0.08 − 4.6]	[0.08 − 4.9]
$I_{del,\alpha}$	[%]	0.605(75)	0.728(85)
$I_{del,\beta}$	[%]	0.185(47)	0.160(48)
$I_{del,\gamma}$	[%]	0.209(62)	0.112(60)

V. CONCLUSIONS

The measured relative intensities of Kx line muonic x rays in μ^3He and μ^4He atoms (see Tables III and V) agree very well with other experiments. Only slight variation due either to the isotope or to the pressure are visible. The stopping power ratio A of helium to deuterium atoms $A = 1.67\left[^{+0.35}_{-0.33}\right]$ is also in good agreement with earlier work [21, 69].

Regarding the $\mathrm{q}^{\mathrm{He}}_{1s}$ probability for a $d\mu$ atom to reach its ground state in a D$_2$ + ^{3}He mixture at two different densities, our results are

$$\mathrm{q}^{\mathrm{He}}_{1s} = (0.882 \pm 0.018) \quad \varphi = 0.0585$$
$$\mathrm{q}^{\mathrm{He}}_{1s} = (0.844 \pm 0.020) \quad \varphi = 0.1680 \qquad (53)$$

in agreement with theoretical calculations for an average $d\mu$ − He collision energy around 8 eV.

As for the $d\mu^3$He molecular formation rate $\lambda_{d^3\mathrm{He}}$ for both our mixtures, our averaged value is

$$\lambda_{d^3\mathrm{He}} = (242 \pm 20)\ \mu\mathrm{s}^{-1} . \qquad (54)$$

Our result agrees very well with the measurement of Maev *et al.* [72], but is in disagreement with the work of Gartner *et al.* [28]. This difference has not yet been understood.

Concerning the radiative decay branching ratio $\kappa_{d\mu\mathrm{He}}$ for $d\mu^3$He, also measured for two different densities of the D$_2$ +^{3} He mixture, the measured values,

$$\kappa_{d\mu\mathrm{He}} = (0.203 \pm 0.014) \quad \varphi = 0.0585$$
$$\kappa_{d\mu\mathrm{He}} = (0.228 \pm 0.012) \quad \varphi = 0.1680 \qquad (55)$$

are the same for both densities, but disagree with the recent results by Augsburger *et al.* [20], $\kappa_{d\mu\mathrm{He}} = (0.301 \pm 0.061)$, measured at a density approximately two times bigger, namely $c_{\mathrm{He}} = 0.0913$.

Finally, the relative intensities of the delayed K series transitions $I^{\mathrm{D/He}}_{del,x}$ of μHe atoms, due to direct ^{3}He muon capture or due to muon transfer from deuterium to helium, after the muons were freed after $d-d$ fusion were also measured. They differ from the prompt relative intensities, probably due to a different primary distribution of excited states.

In conclusion, we were able to measure various interesting characteristics of muon atom (MA) and muonic molecule (MM) processes occurring in pure helium and in D$_2$+^{3}He mixtures with good accuracy. This was possible by exploiting different germanium detectors for γ–ray detection in a wide energy range [3 keV − 10 MeV], silicon Si(d$E - E$) telescope for the detection of charged particles coming from nuclear fusion or nuclear muon capture on ^{3}He and muon decay electron detectors. The self consistent methods increased the reliability of the presented results. Further measurements of quantities such as the muon stopping ratio A, the q_{1s}^{He} probability, and the $\kappa_{d\mu\mathrm{He}}$ branching ratio in wider range of target densities and helium concentrations should significantly improve the accuracy of the corresponding values and clarify the complicated picture of muonic processes occurring in deuterium–helium targets.

Acknowledgments

This work was supported by the Russian Foundation for Basic Research, Grant No. 01–02–16483, the Polish State Committee for Scientific Research, the Swiss National Science Foundation, and the Paul Scherrer Institute.

[1] C. Petitjean, Hyp. Interact. **138**, 191 (2001).
[2] V. M. Bystritsky et al., Yad. Fiz. **58**, 808 (1995), [Phys. At. Nucl. **58**, 746–753 (1995)].
[3] V. M. Bystritsky, Yad. Fiz. **58**, 688 (1995), [Phys. At. Nucl. **58**, 631–637 (1995)].
[4] G. M. Marshall et al., Hyp. Interact. **138**, 203 (2001).
[5] K. Nagamine, Hyp. Interact. **138**, 5 (2001).
[6] C. Petitjean, Nucl. Phys. A **543**, 79c (1992).
[7] G. A. Fesenko and G. Y. Korenman, Hyp. Interact. **101/102**, 91 (1996).
[8] M. P. Faifman and L. I. Men'shikov, Hyp. Interact. **138**, 61 (2001).
[9] J. S. Cohen, RIKEN Review **20**, 8 (1999).
[10] V. E. Markushin and T. S. Jensen, Hyp. Interact. **138**, 71 (2001).
[11] A. Adamczak and M. P. Faifman, Phys. Rev. A **64**, 052705 (2001).
[12] V. E. Markushin, Phys. Rev. A **50**, 1137 (1994).
[13] V. M. Bystritsky et al., Phys. Rev. A **53**, 4169 (1996).
[14] T. S. Jensen and V. E. Markushin, Hyp. Interact. **138**, 113 (2001).
[15] V. P. Popov and V. N. Pomerantsev, Hyp. Interact. **138**, 109 (2001).
[16] V. M. Bystritsky et al., Eur. Phys. J. D **8**, 75 (2000).
[17] V. M. Bystritsky, W. Czapliński, and N. Popov, Eur. Phys. J. D **5**, 185 (1999).
[18] A. V. Kravtsov and A. I. Mikhailov, Phys. Rev. A **49**, 3566 (1994).
[19] S. Sakamoto, K. Ishida, T. Matsuzaki, and K. Nagamine, Hyp. Interact. **119**, 115 (1999).
[20] M. Augsburger et al., Phys. Rev. A **68**, 022712 (2003).
[21] F. Kottmann, in *Muonic Atoms and Molecules*, edited by L. A. Schaller and C. Petitjean (Birkhäuser Verlag, CH–4010, Basel, 1993), pp. 219–233, [Proceedings of the Int. Workshop on Muonic Atoms and Molecules, Ascona].
[22] S. Tresch et al., Phys. Rev. A **58**, 3528 (1998).
[23] B. Lauss et al., Phys. Rev. Lett. **76**, 4693 (1996).
[24] V. M. Bystritsky et al., Zh. Eksp. Teor. Fiz. **84**, 1257 (1983), [Sov. Phys. JETP **57**, 728–732 (1983)].
[25] Y. A. Aristov et al., Yad. Fiz. **33**, 1066 (1981), [Sov. J. Nucl. Phys. **33**, 564–568 (1981)].
[26] S. Tresch et al., Phys. Rev. A **57**, 2496 (1998).
[27] A. V. Kravtsov, A. I. Mikhailov, and V. I. Savichev, Hyp. Interact. **82**, 205 (1993).
[28] B. Gartner et al., Phys. Rev. A **62**, 012501 (2000).
[29] Y. Kino and M. Kamimura, Hyp. Interact. **82**, 195 (1993).
[30] W. Czapliński, A. Kravtsov, A. Mikhailov, and N. Popov, Phys. Lett. A **233**, 405 (1997).
[31] W. Czapliński, M. Filipowicz, E. Guła, A. Kravtsov, A. Mikhailov, and N. Popov, Z. Phys. D **37**, 283 (1996).
[32] W. Czapliński, A. I. Mikhailov, and I. A. Mikhailov, Hyp. Interact. **142**, 577 (2002).
[33] W. Czapliński, E. Gula, and N. Popov, Kerntechnik **67**, 290 (2002).
[34] L. N. Bogdanova, S. S. Gershtein, and L. I. Ponomarev, Pis'ma Zh. Eksp. Teor. Fiz. **67**, 89 (1998), [JETP Lett. **67**, 99–105 (1998)].
[35] F. M. Pen'kov, Yad. Fiz. **60**, 1003 (1997), [Phys. Atom. Nucl. **60**, 897–904 (1997)].
[36] V. F. Boreiko et al., Nucl. Instrum. Methods A **416**, 221 (1998).
[37] P. E. Knowles et al., Hyp. Interact. **138**, 289 (2001).
[38] V. M. Bystritsky et al., Phys. Rev. A (2003), accepted for publication.
[39] E. M. Maev et al., Hyp. Interact. **118**, 171 (1999).
[40] W. Czapliński, A. Kravtsov, A. Mikhailov, and N. Popov, Phys. Lett. A **219**, 86 (1996).
[41] W. Czapliński, A. Kravtsov, A. Mikhailov, and N. Popov, Eur. Phys. J. D **3**, 223 (1998).
[42] L. N. Bogdanova, V. I. Korobov, and L. I. Ponomarev, Hyp. Interact. **118**, 183 (1999).
[43] V. M. Bystritsky and F. M. Pen'kov, Yad. Fiz. **62**, 316 (1999), [Phys. At. Nucl. **62**, 281–290 (1999)].
[44] V. M. Bystritsky, M. Filipowicz, and F. M. Pen'kov, Nucl. Instrum. Methods A **432**, 188 (1999).
[45] R. Schmidt et al., Eur. Phys. J. D **3**, 119 (1998).
[46] P. Hauser, F. Kottmann, C. Lüchinger, and R. Schaeren, in *Muonic Atoms and Molecules*, edited by L. A. Schaller and C. Petitjean (Birkhäuser Verlag, CH–4010, Basel, 1993), pp. 235–241, [Proceedings of the Int. Workshop on Muonic Atoms and Molecules, Ascona].
[47] A. Adamczak, Hyp. Interact. **101/102**, 113 (1996).
[48] F. Kottmann et al., Hyp. Interact. **119**, 3 (1999).
[49] T. Koike, Hyp. Interact. **138**, 95 (2001).
[50] E. Storm and H. I. Israel, Nucl. Data, Sec. A **7**, 565 (1970).
[51] J. H. Hubbell, Int. J. Appl. Radiat. Isot. **33**, 1269 (1982).
[52] E. M. Maev et al., Hyp. Interact. **101/102**, 423 (1996).
[53] A. C. Philips, F. Roig, and J. Ros, Nucl. Phys. A **237**, 493 (1975).
[54] T. Suzuki, D. F. Measday, and J. P. Koalsvig, Phys. Rev. C **35**, 2212 (1987).
[55] J. S. Cohen, Phys. Rev. A **25**, 1791 (1982).
[56] H. P. von Arb et al., Phys. Lett. B **136**, 232 (1984).
[57] M. Eckhause et al., Phys. Rev. A **33**, 1743 (1986).
[58] J. Cohen and M. Struense, Phys. Rev. A **38**, 53 (1988).
[59] W. R. Johnson, Phys. Rev. Lett. **29**, 1123 (1972).
[60] R. Bacher, Z. Phys. A **315**, 135 (1984).
[61] F. Kottmann, in *Second international Symposium on the interaction of muons and pions with matter* (JINR, Dubna, 1987), p. 268.

[62] G. Y. Korenman, S. V. Leonova, and V. P. Popov, Muon Catal. Fusion **5/6**, 49 (1990/91).

[63] M. Bubak and V. M. Bystritsky, JINR Preprint E1–86–107 (1986).

[64] F. J. Hartmann, in *Electromagnetic Cascade and chemistry of exotic atoms*, edited by L. M. Simons, D. Horváth, and G. Torelli (Plenum Press, New York, USA, 1990), p. 23, [Proceedings of the Fifth Course of the International School of Physics of Exotic Atoms, held in Erice, Italy].

[65] D. V. Balin et al., Phys. Lett. B **141**, 173 (1984).

[66] D. V. Balin et al., Pis'ma Zh. Eksp. Teor. Fiz. **40**, 318 (1984), [JETP Lett. **40**, 1112–1114 (1984)].

[67] A. A. Vorobyov, Muon Catal. Fusion **2**, 17 (1988).

[68] G. A. Rinker, Phys. Rev. A **14**, 18 (1976).

[69] V. M. Bystritsky et al., Kerntechnik **58**, 185 (1993).

[70] V. M. Bystritsky et al., Kerntechnik **64**, 294 (1999).

[71] V. M. Bystritsky, A. V. Kravtsov, and N. P. Popov, Muon Catal. Fusion **5/6**, 487 (1990/91).

[72] E. M. Maev et al., Hyp. Interact. **119**, 121 (1999).

[73] V. B. Belyaev, O. I. Kartavtsev, V. I. Kochkin, and E. A. Kolganova, Hyp. Interact. **101/102**, 359 (1996).

[74] S. S. Gershtein and V. V. Gusev, Hyp. Interact. **82**, 185 (1993).

[75] V. B. Belyaev, O. I. Kartavtsev, V. I. Kochkin, and E. A. Kolganova, Phys. Rev. A **52**, 1765 (1995).

[76] V. I. Korobov, V. S. Melezhik, and L. I. Ponomarev, Hyp. Interact. **82**, 31 (1993).

[77] V. Belyaev, O. Kartavtsev, V. Kochkin, and E. A. Kolganova, Z. Phys. D **41**, 239 (1997).

[78] K. Ishida et al., Hyp. Interact. **82**, 111 (1993).